Nonintrusive Load Monitoring and Diagnostics in Power Systems

Steven R. Shaw, *Senior Member, IEEE*, Steven B. Leeb, *Fellow, IEEE*,
Leslie K. Norford, and Robert W. Cox, *Member, IEEE*

***Abstract*—This paper describes a transient event classification scheme, system identification techniques, and implementation for use in nonintrusive load monitoring. Together, these techniques form a system that can determine the operating schedule and find parameters of physical models of loads that are connected to an ac or dc power distribution system. The monitoring system requires only off-the-shelf hardware and recognizes individual transients by disaggregating the signal from a minimal number of sensors that are installed at a central location in the distribution system. Implementation details and field tests for ac and dc systems are presented.**

***Index Terms*—Diagnostics, pattern recognition, system identification.**

I. Introduction

COMPUTATIONAL power and data transmission capabilities for commercial monitoring and control systems have outpaced the problem of putting sensors in all the right places. Obtaining useful information, however, generally requires proper installation, maintenance, and interpretation of a vast collection of sensors—a daunting proposition even if the sensors are mass produced and individually inexpensive.

This paper describes a new platform for transient-based nonintrusive load monitoring that is practical for widespread application. The system uses off-the-shelf hardware, connects to a network, and can be replicated at a cost that is feasible for widespread field evaluation. This paper also describes the development of diagnostic estimation algorithms that are specifically suited to nonintrusive monitoring, where little or no initial parameter information may be available. Last, nonintrusive load monitoring is demonstrated in ac and dc systems.

Nonintrusive load monitors (NILMs) address the "sensor problem" for electrical load monitoring by extracting information about individual loads from a few measurements at an easy-to-access centralized location. At minimum, an NILM can determine the operating schedule of the operating electrical loads in a target system strictly from measurements that are made at a central point in an electric power distribution system [1]–[4]. For example, the NILM can disaggregate and report the operation of individual electrical loads like lights and motors from measurements that are made only at the electrical service entry to a building. It can identify the operation of electromechanical devices in an automobile or other transportation system from similarly convenient measurements. The NILM is capable of performing this disaggregation, even when many loads are operating at the same time. Because the NILM associates observed electrical waveforms with individual kinds of loads, it is possible to exploit modern state and parameter estimation algorithms to remotely verify and determine the condition or "health" of critical loads. (See, for example, [5]–[14] for a historical cross section of reduced-sensor estimation techniques for motors. Reference [15] describes techniques that are suitable for motor parameter estimation from a nonintrusive monitor.) The NILM can also monitor the operation of the electrical distribution system itself, identifying situations where two or more otherwise healthy loads interfere with each other's operation through voltage waveform distortion or power quality problems [16].

Nonintrusive electrical monitoring has been described in [2]–[4] and [17]–[19], among other publications. The systems that are described in these papers can be split into two broad categories—transient and steady-state approaches. Monitors using a steady-state approach [19] discriminate loads by their steady-state power consumption. These monitors have relatively modest computational requirements and have been practical for some time. The transient approach [2], [4] finds loads by examining the full detail of their transient behavior. Implementations of transient NILMs have typically used custom hardware, such as the parallel computer described in [3] or the digital signal processor–personal computer combination in [2]. In this paper, we describe a new platform for transient-based nonintrusive load monitoring that is practical for widespread application. The system is practical because it uses off-the-shelf hardware, connects to almost any kind of information network, and can be replicated at a cost that is feasible for widespread field evaluation. This paper also describes the application of diagnostic estimation algorithms that are specifically suited to nonintrusive monitoring, where little or no initial parameter information may be available about the loads of interest.

Manuscript received September 27, 2005; revised December 18, 2007. This work was supported in part by ONR ESDRC, the National Science Foundation, the National Aeronautics and Space Administration through a Small Business Innovation Research Phase II Award, Textron, Ford Motor Company, and the Grainger and Landsman foundations.

S. R. Shaw is with the Department of Electrical and Computer Engineering, Montana State University, Bozeman, MT 59717 USA.

S. B. Leeb is with the Laboratory for Electromagnetic and Electronic Systems, Massachusetts Institute of Technology, Cambridge, MA 02139 USA.

L. K. Norford is with the Department of Architecture, Massachusetts Institute of Technology, Cambridge, MA 02139 USA.

R. W. Cox is with the Department of Electrical and Computer Engineering, University of North Carolina, Charlotte, NC 28223 USA.

Color versions of one or more of the figures in this paper are available online at http://ieeexplore.ieee.org.

Digital Object Identifier 10.1109/TIM.2008.917179

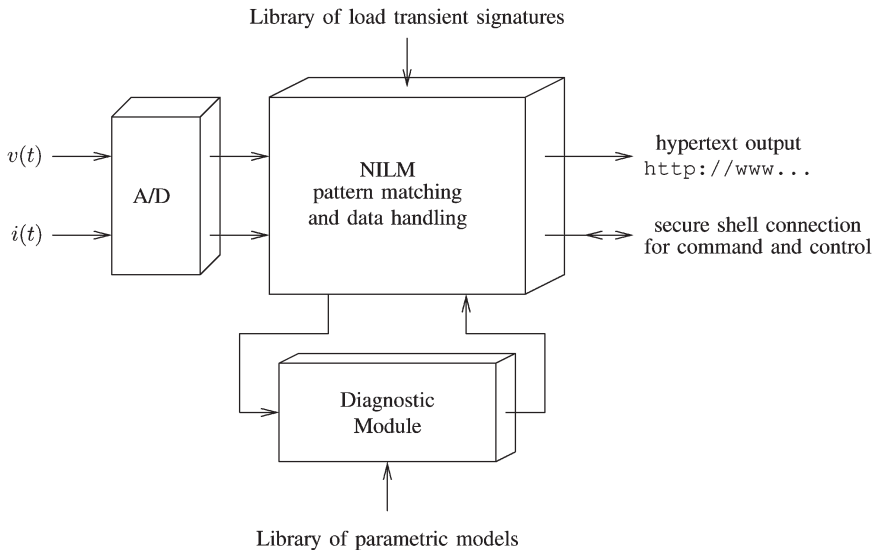

Fig. 1. Overall scheme of the nonintrusive load monitoring and diagnostic instrument (NILM). The NILM measures currents and voltages at a central location, matches transients with respect to a stored library of transient signatures, and performs a more detailed analysis of key transients by identification of parametric load models.

Last, the new NILM platform is demonstrated in the traditional ac electric utility environment as well as in the dc environment of an automobile.

II. Implementation

Fig. 1 shows an overall schematic of the nonintrusive diagnostic and load monitoring system. Physically, the instrument consists of current and voltage sensors that are installed at the target site, a commercial data acquisition card, and a conventional host computer running a version of Linux that is modified to support continuous streaming of information from the analog data acquisition card. The NILM is also connected to an information exchange network, often with a gateway to the Internet. This approach essentially eliminates two key problems—retrieving data and updating software. Our implementation uses the hypertext transfer protocol to supply information to client machines on the network. A secure shell connection is used for upgrading software, reconfiguration, and most system administration tasks. The secure shell connection can also be used for specialized or infrequent experiments, such as collecting training data or high-sample-rate transient studies. One disadvantage of the approach in Fig. 1 is the possibility that the instrument might be compromised by unauthorized users. This possibility is minimized by disabling all Internet services on the host computer, except those that are needed to function as a remote instrument.

The software underlying the system in Fig. 1 is organized as a series of functional modules, beginning with preprocessing. Preprocessing converts raw voltage and current data from the A/D interface to a standard format. Preprocessing may also involve mathematical transforms to simplify the discrimination of different transients. Preprocessing requirements depend on whether the NILM is installed in an ac or dc environment and on the encoding scheme that is used by the data acquisition interface. Event classification follows preprocessing and typically involves fitting stored load transient "fingerprints" to incoming transient data. Following event classification, the NILM routes or dispatches raw data, preprocessed data, and data from event classification to a reconfigurable array of client processes. Client processes may include Internet interfaces that make the results of event classification available on the Web, logging programs, and diagnostic programs that obtain estimates of the parameters of models describing observed transients. The section concludes with the system identification procedures that are used in the diagnostic part of the NILM.

A. Preprocessing

The purpose of preprocessing is to transform the measurements so that it is easy to match transients. In an ac system, some preprocessing to extract useful task-related features is usually necessary. Estimates of spectral envelope coefficients [2], [20], [21] are particularly useful. Spectral envelopes are short-time averages of the harmonic content of a signal, e.g., a signal $x(t)$ of current observed by the NILM. The in-phase spectral envelopes a_k of x are

$$a_k(t) = \frac{2}{T}\int_{t-T}^{t} x(\tau)\cos(k\omega\tau)d\tau \tag{1}$$

where k is the harmonic index. Similarly, the quadrature spectral envelopes b_k are

$$b_k(t) = \frac{2}{T}\int_{t-T}^{t} x(\tau)\sin(k\omega\tau)d\tau. \tag{2}$$

These spectral envelopes may be recognized as the coefficients of a time-varying Fourier series of the waveform $x(t)$ [4]. For transient event detection on the ac utility, the time reference is adjusted so that the term $\cos(k\omega\tau)$ in (1) is phase locked to the

voltage measurement. The window T is typically one or more periods of the fundamental frequency of the voltage waveform. For a_k and b_k that are computed under these conditions, the spectral envelopes are called $P_k = a_k$ and $Q_k = b_k$. Notice that steady-state spectral envelopes P_1 and Q_1 correspond to the conventional definitions of real and reactive power, respectively. In a dc system with a constant bus voltage, current measurements are proportional to the power consumed by a load. Since loads that are intended for different tasks differently consume power, the current transients in a dc system are useful for distinguishing different loads.

Short-time Fourier transforms are used for computing spectral envelope coefficients in the present NILM implementation. Current and voltage data are resampled by linear interpolation to provide power-of-two samples per period. In our case, 128 samples per period were used. A fast Fourier transform (FFT) was applied to the resampled current and voltage, resulting in transformed vectors I and V. Note that since i and v are real, their discrete Fourier transforms (DFTs) are conjugate symmetric and could be computed using half the number of points. We use the notation V_1 to indicate the normalized negative-frequency coefficient of the FFT of v corresponding to the first harmonic. Although the data input to the FFT is resampled, there is no means to control the phase of the voltage relative to the window that is used in the FFT. Therefore, the first harmonic coefficient V_1 will, in general, have some angle θ. To obtain the spectral envelope components of the current relative to this voltage, the complex coefficients I_k are rotated by θ to obtain the correct phase relationship to the voltage. In particular, we define a complex phase correction, i.e.,

$$\phi = e^{-j\theta} \tag{3}$$

and compute phase-corrected spectral envelope estimates as follows:

$$I'_k = \phi^k I_k \approx P_k + jQ_k. \tag{4}$$

As an example, consider the case of a resistive load where the current is a scaled copy of the voltage. Because the phase of the FFT data window with respect to the voltage is unknown, V_1 and I_1 will share some angle θ. Applying the rotation $\phi = e^{-j\theta}$ to I_1 and V_1 yields phase-corrected V'_1 and I'_1 that are real. For a resistive load, the real-power spectral envelope coefficient $P_1 \approx \mathrm{Re}\{P'_1\}$ is nonzero, and the reactive power coefficient $Q_1 \approx \mathrm{Im}\{I'_1\}$ is zero.

The spectral envelope estimates that are obtained using this procedure are not identical to those obtained using (1) and (2) or the various preprocessors described in [2] and [4]. However, the estimates retain qualitative features that are useful for pattern matching, including a close correspondence to envelopes of the real and reactive power consumed by a load.

As an example, Fig. 2 shows a typical short-time Fourier transformed spectral envelope computation for the free acceleration startup of a fractional horsepower three-phase induction machine. The spectral envelope transient strongly reflects the underlying physics. At the beginning of the transient, the machine draws power to accelerate the rotor. The motor consumes less power in steady state.

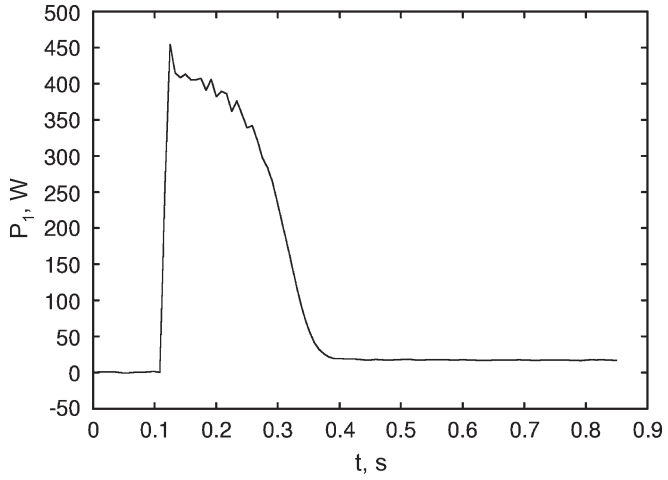

Fig. 2. Spectral envelope estimate of P_1 for a fractional horsepower induction machine.

B. Event Classification

Electrical load transients in an incoming stream of data are classified by comparison to a library of transient signatures. Load transient signatures, or exemplars, are typically extracted from measured data during a training phase [22]. It is generally not necessary to record data for all possible loads because different loads within a class tend to have spectral envelope transients that are similar up to scale factors in duration and amplitude [20].

A change-of-mean event detector triggers the process of matching an observed transient with previously stored exemplars. This is in contrast to the system described in [20], which scans every incoming point for patterns. If an exemplar is accepted as a fit to some portion of the incoming data, associated events are removed from the list of detected events to prevent them from being claimed by other patterns. During matching, complicated exemplars with the most sections are tried before simpler exemplars. This prevents shorter exemplars from claiming events that belong to a larger exemplar.

Exemplars are parameterized so that they can match different transients within a class of loads. Fig. 3 shows the associated degrees of freedom for an exemplar consisting of two sections, with shape vectors s_1 and s_2. The origin of each section can be shifted in time by k and by an associated offset b_k, as in Fig. 3. All the sections in the exemplar are subject to an overall gain α. Sections need not consist of an uninterrupted sequence of points—each of N sections in the exemplar is defined by a shape vector s and a time vector t. Exemplars are currently selected by hand from observed data to capture the relatively high-derivative and most repeatable parts of a transient: a task that could be automated. If the exemplars are properly designed, the sections of two exemplars may interleave during matching, allowing the transient classifier to tolerate a limited degree of transient overlap. Numerically, exemplars are matched to incoming data by individual sections rather than as a global

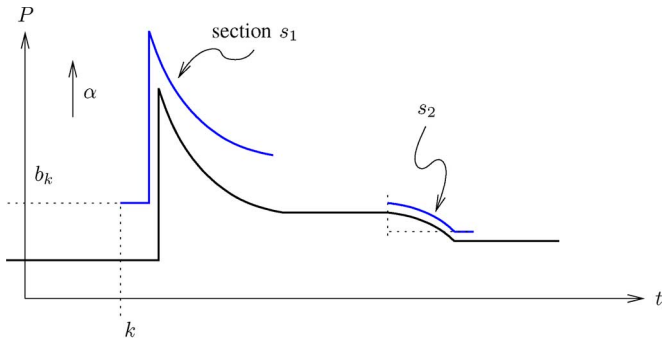

Fig. 3. Pattern matching scheme. The exemplar has two sections with shape vectors s_1 and s_2. An overall scale factor α and a time shift k and offset b_k for each section are determined to provide the best fit to the observations.

problem for the entire exemplar. In particular, the least squares problem

$$\begin{pmatrix} s[1] & 1 \\ \vdots & \vdots \\ s[M] & 1 \end{pmatrix} \begin{pmatrix} a_k \\ b_k \end{pmatrix} = \begin{pmatrix} d\left[T_e + t[1] + k\right] \\ \vdots \\ d\left[T_e + t[M] + k\right] \end{pmatrix} \tag{5}$$

is solved for each M-point section over a range of the sample time shift k. In (5), T_e is the index of the event, d is the incoming data, and s and t are the shape and time vectors, respectively, describing the section. Final values of k, a_k, and b_k are assigned according to the best least squares fit over the attempted values of k. For the jth section of the exemplar, a vector

$$r_j = \begin{pmatrix} d\left[T_e + t[1] + k\right] \\ \vdots \\ d\left[T_e + t[M] + k\right] \end{pmatrix} - b_k \tag{6}$$

is stored using final values of k and b_k that are found for that section. The overall gain α of the N-section exemplar is determined by solving

$$\begin{pmatrix} s_1 \\ \vdots \\ s_N \end{pmatrix} \alpha = \begin{pmatrix} r_1 \\ \vdots \\ r_N \end{pmatrix} \tag{7}$$

where the shape vector s_j is the jth section in the exemplar. Of the collection of exemplars, the exemplar offering the smallest residual norm per number of points is selected as the best fit. If the residual norm per number of points exceeds a threshold, the transient is left unclassified.

C. Event Dispatch

A reconfigurable array of postprocessing and display programs postprocesses successfully classified transients. Any number of postprocessing modules can operate at run time. These postprocessing programs include simple scripts that record contact times and classifications to disk, X-windows programs that display contact information graphically, and in-memory Web servers that prepare and serve HTML and graphics descriptions of the transient and its classification.

The ability to reconfigure monitoring and diagnostics features at run time facilitates the implementation of a variety of special-purpose Web-accessible load and power-quality instruments with little programming effort. Another important advantage of the modular event-dispatch model is that post-processing programs can be implemented in the most efficient language available. A typical configuration of the event dispatcher might include a logging program recording textual contact information from the tag queue to a disk, a graphics display program converting information from the graphic queue to HTML and portable network graphics images for a Web server, and a few diagnostic programs that are written for key loads of particular interest. Diagnostic programs might be independently connected to logging programs or additional graphic display programs.

III. Experimental Results

The nonintrusive load monitoring and diagnostics system has been installed in a variety of locations outside the laboratory. These locations include commercial buildings in California, an experimental building in Iowa, commercial facilities in Massachusetts, a collection of U.S. Coast Guard and U.S. Navy operational vessels and land-based test facilities, and a dormitory on the Massachusetts Institute of Technology campus. For the purposes of this paper, we have picked three scenarios that highlight the capabilities of the instrument in ac and dc environments for monitoring and diagnostic applications.

A. Automotive Transient Classification and Identification

The nonintrusive load monitoring and diagnostics system was installed in a 1986 Chevrolet Nova for field testing in a dc power delivery system. The installation was accomplished by installing a number of current sensors at strategic locations in the engine compartment. These sensors are connected to an A/D converter and a portable computer in the passenger compartment of the vehicle. Results can be monitored at the console of the portable computer, although, in principle, a radio modem or cellular data approach could be used for remote monitoring.

1) Instrumentation: Fig. 4 shows a working model of the electrical system in the test vehicle. Three LEM LA55-P active Hall-effect current sensors were used to measure the aggregate current $i_1 + i_2 + i_3$ due to electrical loads in the vehicle. The sensor response was digitized using a 12-bit 150-Hz A/D converter that is connected to the serial port of a portable computer. This choice of measurements eliminates currents that are returned to the engine block, including the current that is required for the starter motor and the ignition system, and the charging current between the battery and the alternator. Although these currents might contain interesting information, they are of different character—they have either a considerably higher magnitude or frequency—than other transients in the vehicle.

2) Transient Classification: Loads in the car are mostly lights and motors. For testing, the monitor was supplied with nine exemplars for loads, including the hazard lights, the brake lights, the fan, the headlights, and the cigarette lighter. Of these loads, scaled exemplars for incandescent lightbulbs proved to

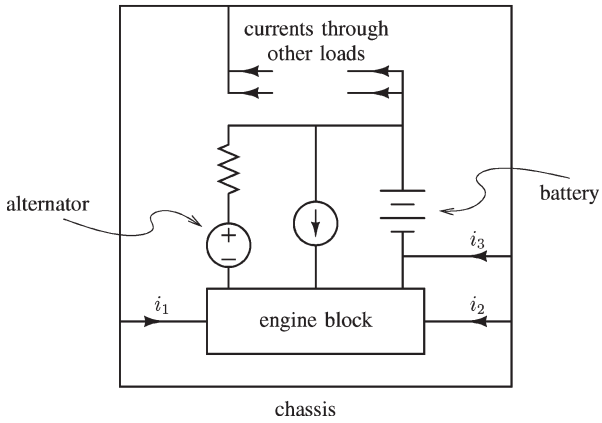

Fig. 4. Working model of a car electrical system, including measured currents i_1, i_2, and i_3.

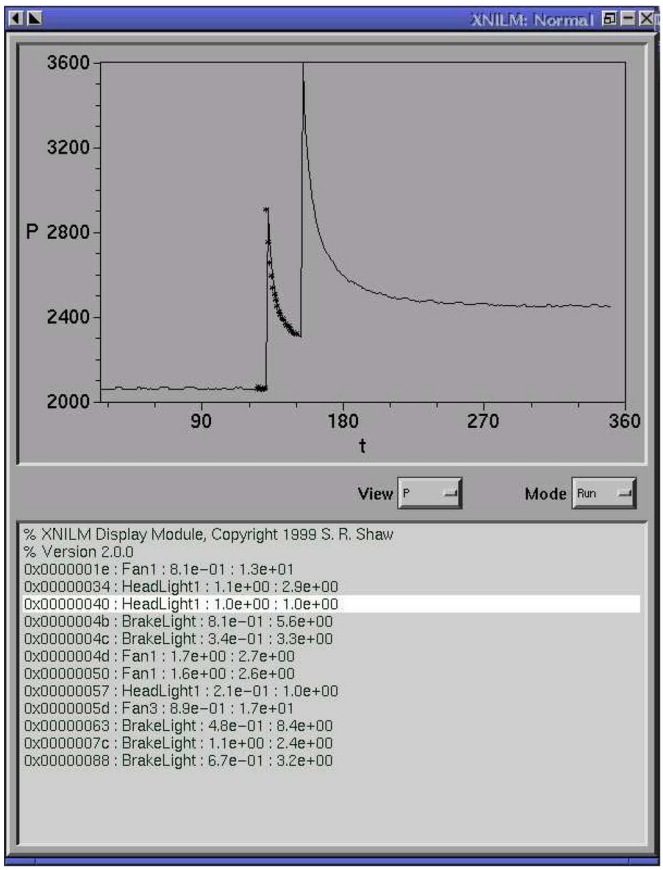

Fig. 5. X-windows NILM interaction showing detection of a headlight transient. Solid lines in the graph are measured data; the points show the fit of the exemplar to the transient.

be very similar. This is not surprising because a large incandescent lightbulb performs the same physical task as a small lightbulb. Exemplar scale factor information could be used, for example, in an application requiring that the headlights be distinguished from the dome light.

Fig. 5 shows a correctly classified headlight transient. Turning on the headlights actually results in two transients, as can be seen in Fig. 5. This is because the first position on the headlight control activates the parking lights, and the second position activates the headlights. Fig. 5 is the output of a graphical display program that is connected to a queue on the event dispatcher.

3) Ventilation System Parameter Identification: In addition to classifying a variety of transients in the automobile, the nonintrusive monitor was also configured to dispatch transients due to the ventilation fan to a parameter identification program. The passenger compartment ventilation system is particularly interesting because it is essentially a ducted fan that is connected to a user-reconfigurable mechanical system of vents, louvers, and pipes. No direct electrical signal is available to provide information about the state of the mechanical settings. However, electrical transients from the fan motor and an appropriate model can be used to extract information about the attached mechanical system.

We model the ventilation system as a dc motor that is connected to a ducted fan. A series resistance R captures the motor and wire resistance and the ballast resistor that is used to set the fan speed. Also included in the model are the inertia J, the motor constant K, and a drag coefficient β_f. The inertia J lumps the effects of the components on the shaft of the motor with the air mass coupled to the shaft through the fan. The mechanical equation of motion for this system is

$$J\frac{d\omega_r}{dt} = T_e - \beta_f\omega_r^2 \tag{8}$$

where ω_r is the shaft speed, and T_e is the torque of the electric origin, i.e.,

$$T_e = Ki_m. \tag{9}$$

Noting that

$$i_m = \frac{v_m - K\omega_r}{R} \tag{10}$$

(8) may be rewritten as follows:

$$J\frac{d\omega_r}{dt} = K\frac{v_m - K\omega_r}{R} - \beta_f\omega_r^2. \tag{11}$$

This system apparently has four parameters; however, under the substitution $x = (JR/K)\omega_r$, it can be rewritten as

$$\frac{dx}{dt} = v_m - \alpha_1 x - \alpha_2 x^2 \tag{12}$$

with observations

$$i_m = \alpha_3(v_m - \alpha_1 x). \tag{13}$$

In terms of the original parameters

$$\alpha_1 = \frac{K^2}{RJ} \tag{14}$$

$$\alpha_2 = \frac{\beta_f K}{J^2 R} \tag{15}$$

$$\alpha_3 = \frac{1}{R}. \tag{16}$$

TABLE I
COMPARISON OF PARAMETER ESTIMATES FOR AUTOMOBILE VENTILATION SYSTEM WITH SELECTOR ON "VENT" OR "HEAT"

Scenario	Parameters			Fit Quality
	α_1	α_2	α_3	$\|r\|/\|I\|$
Fresh/Vent	.20	.094	.46	2.5e-2
Fresh/Heat	.12	.021	.44	4.2e-2
Recirc/Vent	.15	.077	.44	2.5e-2
Recirc/Heat	.11	.022	.44	2.6e-2

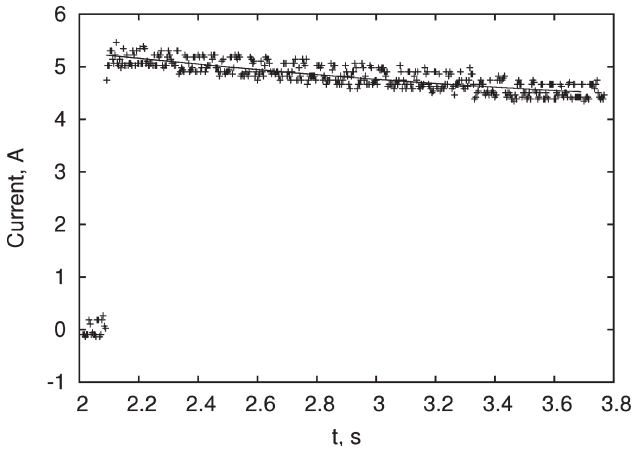

Fig. 6. Measured data (points) and fit of (13) for the recirculation/heat scenario in Table I.

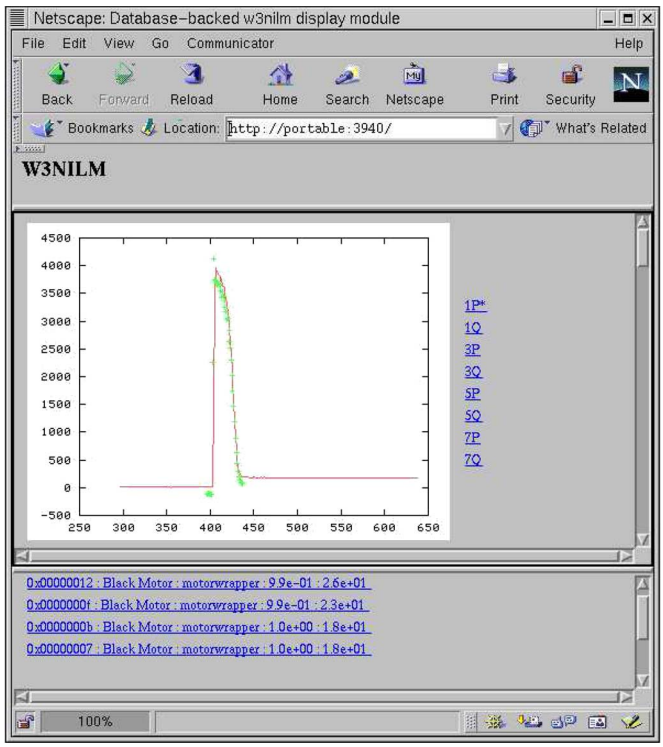

Fig. 7. Web browser showing detection of induction motor transients in an ac service. Solid lines in the graph are spectral envelope data; the points show the fit of the exemplar to the transient.

The parameters for this model were identified by adjusting the parameters to minimize the residual

$$r = I - \hat{i}_m(\alpha_1, \alpha_2, \alpha_3) \tag{17}$$

where I is the measured current, and $\hat{i}_m(\alpha_1, \alpha_2, \alpha_3)$ is the modeled current obtained from (13).

Using the techniques in [23] and the data dispatched from classified transients, parameters were obtained for four configurations of the ventilation system. The estimated parameters, which have been summarized in Table I, make a good physical sense. Switching from vent to heat involves changing the airflow from short pipes to longer pipes. In terms of the natural parameters of the system, R and K might be expected to stay the same; the fan motor is unchanged, and the fan was run at the same set speed. In terms of the identified parameters, α_3 should stay the same. However, the air mass that is coupled to the fan should increase as the duct length increases; therefore, the lumped inertia J should increase. Larger J corresponds to smaller α_1. Based on this physical reasoning, α_1 in Table I should be smaller for the "heat" settings than the "fresh" settings. Also, the estimates of α_3 in Table I should be roughly the same. The parameters in Table I are consistent with these expectations (see also Fig. 6).

B. AC Transient Classification and Identification

As an ac system application example, the nonintrusive monitor was connected to a single phase of a three-phase 120 V ac line-neutral service. In this case, instrumentation consisted of a standard personal computer that is connected to a local network, an Advantech PCL818L A/D interface, and an LEM LA55-P current transducer. With the exception of the device driver and spectral envelope preprocessing routines, the software was identical to that used in the automobile.

1) Transient Classification: A variety of loads are present on the monitored phase, including induction machines, a computer, an instant start, a compact fluorescent, a rapid start, and incandescent lights. For testing purposes, the transient classifier was supplied with a set of eight exemplars, including at least one exemplar per load class. These exemplars were generated using measured data that are collected and modified by hand with the aid of a MATLAB/octave script that is written for this purpose.

Fig. 7 is an example of the Web-based output capabilities of the nonintrusive classifier and illustrates the classification of a motor turn-on transient in an ac service. Solid lines show spectral envelope data, whereas the points indicate the fit of the exemplar to the data. The tag data, which is shown in the bottom part of Fig. 7, include the text "motorwrapper." This indicates to the event dispatcher that a parametric model, i.e., "motorwrapper," is available for further identification of the classified transient.

2) Induction Machine Parameter Identification: A three-phase, 200-W, 1725-r/min Robins and Myers induction machine that is connected to a three-phase 120 VAC line-to-neutral service was used to test the combination of nonintrusive classification and identification in an ac situation.

The dynamics of a three-phase induction machine can be modeled according to the synchronously rotating coordinate

TABLE II
PARAMETER ESTIMATES FOR INDUCTION MOTOR CLASSIFICATION AND IDENTIFICATION TESTS. SINCE $K \propto (1/J)$, K SHOULD BE SMALLER IN LOADED CASES THAN WHEN UNLOADED

Scenario		Parameters						Fit Quality
Dataset	Load	r_s	r_r	L_m	L_l	K	β	$\|r\|/\|I\|$
1	Y	11.6	5.74	.778	.0197	613	.00191	2.5e-5
2	Y	11.7	5.75	.776	.0195	613	.00189	2.6e-5
3	N	11.8	5.69	.761	.0196	656	.00188	3.0e-5
4	N	11.6	5.74	.774	.0195	638	.00189	2.9e-5
5	N	11.6	5.73	.775	.0195	630	.00189	2.8e-5
6	N	11.6	5.72	.770	.0196	637	.00189	2.5e-5
7	Y	11.7	5.73	.774	.0194	610	.00190	2.5e-5
8	Y	11.7	5.75	.775	.0194	618	.00190	2.6e-5
9	Y	11.7	5.75	.773	.0194	613	.00190	2.6e-5
10	Y	11.7	5.74	.774	.0194	610	.00190	2.9e-5
11	N	11.6	5.77	.772	.0196	637	.00188	2.9e-5
12	N	11.6	5.76	.772	.0197	642	.00189	2.6e-5

frame or dq-space equations, i.e.,

$$\frac{d}{dt}\begin{pmatrix}\lambda_{qs}\\ \lambda_{ds}\\ \lambda_{qr}\\ \lambda_{dr}\end{pmatrix} = \begin{pmatrix}v_{qs}\\ v_{ds}\\ 0\\ 0\end{pmatrix} - \begin{pmatrix}r_s i_{qs} + \omega_0 \lambda_{ds}\\ r_s i_{ds} - \omega_0 \lambda_{qs}\\ r_r i_{qr} + (\omega_0 - \omega_r)\lambda_{dr}\\ r_r i_{dr} - (\omega_0 - \omega_r)\lambda_{qr}\end{pmatrix} \quad (18)$$

where ω_0 is the frequency of excitation at the stator, ω_r is the rotor speed, and λ's are the flux linkages with rotor quantities and parameters as reflected to the stator [24], [25]. The voltages v_{qs} and v_{ds} are the excitation at the stator, and r_r and r_s are the resistances associated with the rotor and the stator, respectively. The flux linkages and currents are related according to

$$\lambda_{qs} = L_l i_{qs} + (L_l + L_m)(i_{qs} + i_{qr})$$

$$\lambda_{ds} = L_l i_{ds} + (L_l + L_m)(i_{ds} + i_{dr})$$

$$\lambda_{qr} = L_l i_{qr} + (L_l + L_m)(i_{qs} + i_{qr})$$

$$\lambda_{dr} = L_l i_{dr} + (L_l + L_m)(i_{ds} + i_{dr})$$

where L_l is the leakage inductance, and L_m is the magnetizing inductance. Mechanically, a friction and mass mechanical model was assumed and modeled in terms of the rotor speed as follows:

$$\frac{d}{dt}\omega_r = 3K(\tau - \beta\omega_r) \quad (19)$$

where $\tau = \lambda_{qr} i_{dr} - \lambda_{dr} i_{qr}$ is proportional to the torque of the electrical origin, and K is a parameter that is inversely proportional to the inertia, which is connected to the motor shaft. Since only a single phase of the motor current was available for measurement, the lab-frame output equation

$$i_{as} = i_{qs}\cos(\omega_0 t + \phi) + i_{ds}\sin(\omega_0 t + \phi) \quad (20)$$

was used, where ϕ is the angle in the line cycle when the machine was switched on. Parameters were determined by least squares minimization of the residual

$$r = I - \hat{i}_{as}(\mu) \quad (21)$$

with measurements I and parameter vector

$$\mu = (r_s \quad r_r \quad L_m \quad L_l \quad K \quad \beta)'. \quad (22)$$

In the ac nonintrusive monitor configuration, the preprocessor phase-locks in software to compute spectral envelopes. The measured data consist of current and voltage waveforms that are resampled to a power of two points per line cycle. In this case, the sampling rate of I was about 7.7 kHz or 128 points per line cycle.

The NILM was configured to recognize the transient of the test motor, as in Fig. 7, and dispatch the associated measurements to an identification program to find the parameters. During a series of runs, a small pulley was either added or removed from the shaft to test whether the diagnostics could detect a change in the system. This test simulates a situation where changes in the mechanical load of a nonintrusively monitored motor are of diagnostic interest. Results are given in Table II. Because the same motor was used for each test, the electrical parameters and β in Table II should be essentially the same for all 12 trials. In contrast, the estimates for K should reveal whether the pulley was attached to the shaft. Since $K \propto (1/J)$, the trials with the pulley attached should have smaller values of K. In Table II, the average K value for the loaded case is about 613 with a sample standard deviation of 3. The extreme unloaded value is 618: a difference of less than 1%. The average K value for the unloaded tests is about 640, with a sample standard deviation of less than 9. The last column of Table II shows the relative error of the residual as a measure of the quality of fit. Given the variation across the experiments, three significant figures are appropriate for the electrical parameters and β. A dc test of the stator at the motor terminals yielded an r_s of about 9.7 Ω, providing additional assurance that the values in Table II are reasonable. Part of the discrepancy in the r_s value is due to the resistance of the wiring that separates the NILM installation location from the motor terminals. In addition, a high-current line-frequency startup transient may lump losses in r_s that are not present in a low-current dc test. Typical agreement between the measured data and the model is shown in Fig. 8. In contrast to the high-noise vehicle monitoring problem, the differences between prediction and measurement in Fig. 8 appear to be modeling errors.

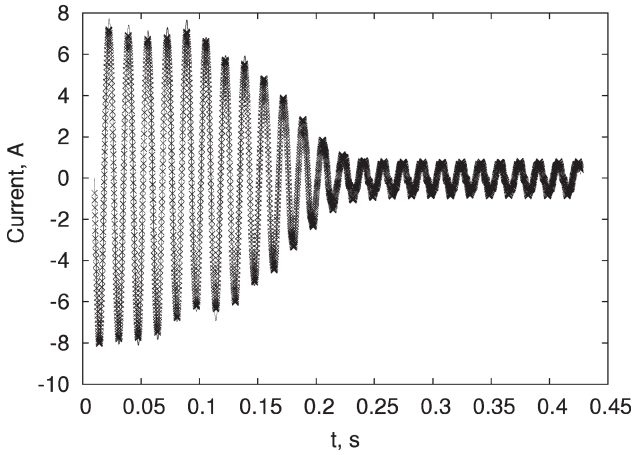

Fig. 8. Measured data (points) and fit of (20) for data set 12 in Table II.

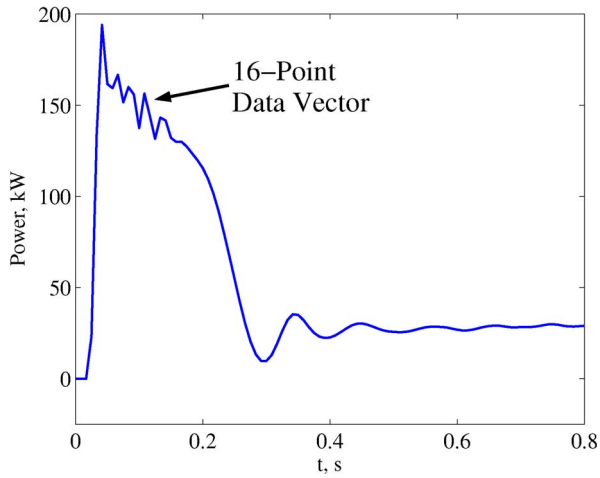

Fig. 9. Real power that is drawn during a typical ASW pump start. The relative location of the data vector shown here was the same for each of the pump starts. The data shown here were sampled at 120 Hz: the nominal output rate of the NILM preprocessor.

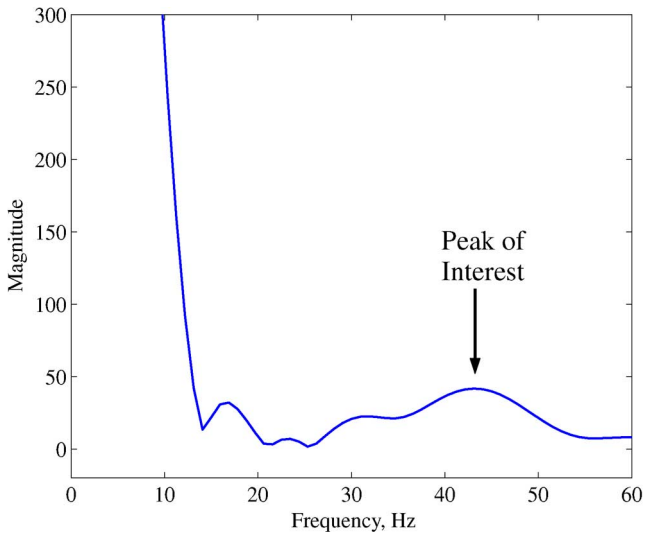

Fig. 10. Magnitude of the frequency spectrum of the windowed data vector shown in Fig. 9.

C. AC Electromechanical Diagnostics

Numerous systems that are aboard modern naval vessels use couplings to link pumps and other mechanical systems to their driving motors. The failure of such couplings can have a drastic impact on mission capability. For instance, the auxiliary seawater (ASW) cooling system on the United States Coast Guard Cutter Seneca has two pumps that are both linked to induction motors via flexible couplings. These couplings have shown a tendency to fail over time. The ASW system provides cooling water to vital shipboard loads, such as the diesel generators. Thus, coupling failure can cause machinery to overheat and sustain damage. This section details the specifics of the problem that was observed aboard the Seneca, and it presents a prognostic metric that the NILM can compute as a postprocessing dispatch to identify an impending problem.

1) Preliminary Analysis of Seneca ASW Data: To investigate the effects of coupling failure in the Seneca ASW system, a fresh standard-issue United States Coast Guard coupling was installed, and the pumps were cycled on and off several times. During each start, an NILM monitored the power that is delivered to the pumps. An example of the real power that is drawn during an ASW pump start is shown in Fig. 9.

Upon comparing the power that is drawn during each of the various pump starts, it was noticed that the amount of high-frequency "ripple" that is present in the real-power spectral envelope transient increased as the coupling progressively failed. To study this trend, we extracted a data vector from each waveform, as shown in Fig. 9, and computed its frequency spectrum using a 128-point windowed DFT. Fig. 10 displays the magnitude of the resulting frequency spectrum for the data vector that is highlighted in Fig. 9.

A resonance in the mechanical coupling subsystem interacting with the motor can be predicted by physical modeling to appear near 44 Hz for the Seneca ASW system. We anticipated that the progressive failure would cause variations in the damping and stiffness coefficients, which, in turn, would cause variations in the amplitude of the observed oscillations. The physical model and an illustrative simulation are presented in [26] and [27]. Analyzing the frequency content of the power that is drawn by the motor over successive starts, we found that the amplitude of a spectral peak located at approximately 44 Hz indeed progressively increased as the coupling failed. This behavior can be seen in Fig. 11. Fig. 12 displays photographs of the coupling over a life cycle of use.

2) Diagnostic Indicator: Our experimental observations and analytical results suggest that a way to diagnose deteriorating coupling conditions is to trend the behavior of the high-frequency spectral peak that is associated with the coupling. Our preliminary diagnostic software uses the three key steps listed below.

- DFT computation: First, we compute the DFT of a windowed segment of the real power spectral envelope that is drawn during a motor start.
- Peak frequency location: The DFT samples spanning the frequency band from 30 to 60 Hz are searched to find the location of the largest spectral peak in that band.

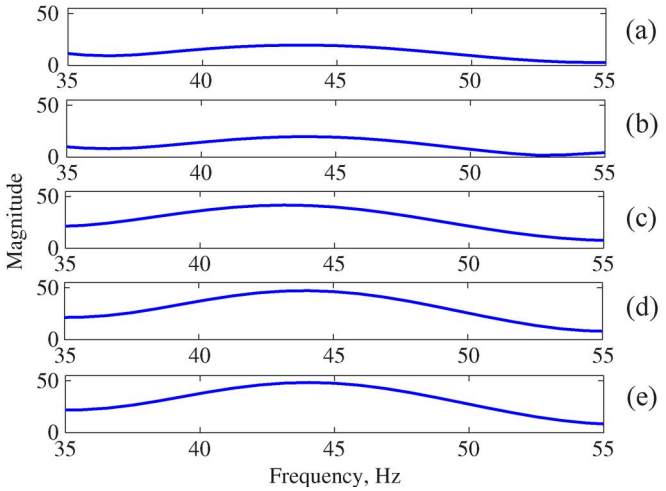

Fig. 11. Details of the high-frequency segment of the magnitude of the frequency spectrum of P_1 during several pump starts. The top trace was recorded after one of the first starts with a fresh coupling, and the bottom trace was recorded during the start before the coupling finally completely failed. Each start is designated by a letter written to the right of the corresponding trace.

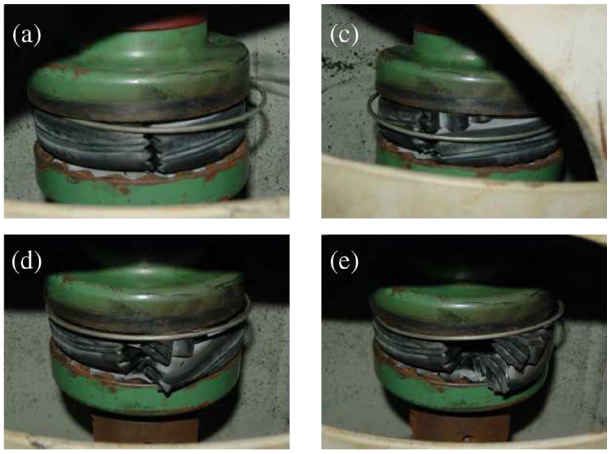

Fig. 12. Photographs showing the state of the coupling over a life cycle of use. The letters in each photograph correspond to the start letters in Fig. 11. Note the tearing that develops as the coupling deteriorates.

- Diagnostic indicator computation: We compute the energy in a band of frequencies centered around the spectral peak (see [26]).

Table III summarizes the diagnostic indicator values corresponding to each of the actual ASW pump starts that are used to form Fig. 11. Note that this value significantly increases between starts B and C. When this behavior is observed in the field, the NILM can immediately alert the engineer officer. This would enable inspection of the coupling well before mission-critical failure.

IV. Discussion

We are on the verge of an era of "sensor bloat." It has become almost second nature to expect that local or global networks and information exchanges will be used to connect arrays of sensors with ever-increasing quantities of analysis software. The design complexity and the monolithic integration afforded by modern electronics have led to a "more is better" attitude in the construction of control and monitoring systems. This trend is apparent in diagnostic, control, and monitoring devices in all areas, particularly including building energy management systems, transportation systems, and industrial process controllers.

TABLE III
Coupling Diagnostic Indicator Value for Each of the Starts

Start Letter (see Fig. 12)	Diagnostic Value
A	23.7
B	22.7
C	112.5
D	139.2
E	146.2

The value of physical simplicity should not be overlooked. Complex arrays of monitoring sensors tend to increase the difficulty and the cost of installation, particularly for short-term or temporary monitoring. Larger arrays of less-expensive sensors may diminish overall reliability and require the collation of data streams from different points.

The nonintrusive monitor that is presented in this paper minimizes the sensor requirement and provides a flexible platform for diagnostic and control monitoring for almost any electromechanical system or plant. The NILM is quick to install and physically reliable because of its relative hardware simplicity. The NILM's ability to associate observed electrical waveforms with the operation of particular devices makes it a perfect foundation for diagnostic and power quality monitoring systems using state and parameter estimation techniques, as described in this paper and its references.

There are, of course, practical limits to the NILM's ability to disaggregate load behavior from aggregated electrical measurements. At some level of aggregation, a high level of simultaneous or nearly simultaneous transient events will make complete disaggregation practically impossible. The rate of event generation at a particular monitoring point determines, in part, the likely success of the NILM in a given application. Our preliminary field tests with the NILM have indicated excellent performance with low rates of event detection errors in typical buildings and transportation systems. Also, the performance of the NILM may degrade fairly gracefully as the rate of event generation increases. Significantly large transients or transients with particularly distinctive features may be detectable, even in a very complex aggregated signal. The NILM may be able to extract these important features, even when the monitor is installed in a location that precludes the exhaustive classification of all events.

The difference between the nonintrusive capabilities that are exemplified by the NILM and conventional monitoring can be viewed as a design tradeoff. Ignoring the possibility of sensor hardware failure, the highest confidence in event and diagnostic detection and recognition will be achieved with individual sensors for every load of interest. The greatest ease of installation, the greatest overall monitoring system reliability, and the lowest cost are probably associated with a nonintrusive monitoring approach. A designer of a monitoring system can, therefore, use the nonintrusive approach to make a flexible tradeoff in expense, reliability, and detection error by

determining an appropriate level of "nonintrusiveness" for any monitoring system.

ACKNOWLEDGMENT

The authors would like to thank Dr. N. Lupton and Dr. J. Rodriguez of NEMOmetrics, LLC, and Prof. G. Verghese, Prof. J. Kirtley, and Prof. J. White of the Massachusetts Institute of Technology for their valuable advice and support.

REFERENCES

[1] S. R. Shaw, "System identification techniques and modeling for nonintrusive load diagnostics," Ph.D. dissertation, Mass. Inst. Technol., Cambridge, MA, Feb. 2000.
[2] S. R. Shaw, C. B. Abler, R. F. Lepard, D. Luo, S. B. Leeb, and L. K. Norford, "Instrumentation for high performance nonintrusive electrical load monitoring," *ASME J. Solar Energy Eng.*, vol. 120, no. 3, pp. 224–229, Aug. 1998.
[3] U. A. Khan, S. B. Leeb, and M. C. Lee, "A multiprocessor for transient event detection," *IEEE Trans. Power Del.*, vol. 12, no. 1, pp. 51–60, Jan. 1997.
[4] S. B. Leeb, S. R. Shaw, and J. L. Kirtley, "Transient event detection in spectral envelope estimates for nonintrusive load monitoring," *IEEE Trans. Power Del.*, vol. 10, no. 3, pp. 1200–1210, Jul. 1995.
[5] K. Hurst and T. Habetler, "Sensorless speed measurement using current harmonic spectral estimation in induction machine drives," in *Proc. 25th Annu. IEEE Power Electron. Spec. Conf.*, 1994, vol. 1, pp. 10–15.
[6] K. R. Cho, J. H. Lang, and S. D. Umans, "Detection of broken rotor bars in induction motors using parameter and state estimation," *IEEE Trans. Ind. Appl.*, vol. 28, no. 1, pp. 702–708, May/Jun. 1992.
[7] A. Bellini, A. de Carli, and M. L. Cava, "Parameter identification for induction motor simulation," *Automatica*, vol. 12, no. 4, pp. 383–386, Jul. 1976.
[8] A. Consoli, L. Fortuna, and A. Gallo, "Induction motor identification by a microcomputer-based structure," *IEEE Trans. Ind. Electron.*, vol. IE-34, no. 4, pp. 422–428, Nov. 1987.
[9] T. Irisa, S. Takata, R. Ueda, T. Sonoda, and T. Mochizuki, "A novel approach on parameter self-tuning method in ac servo system," in *Proc. IFAC Symp. Control Power Electron. Electr. Drives*, 1984, pp. 41–48.
[10] H. Kubota, K. Matsuse, and T. Fukao, "New control method of inverter-fed induction motor drive by using state observer with rotor resistance identification," in *Conf. Rec. IAS Annu. Meeting*, 1985, pp. 601–606. 85CH2207-9.
[11] D. Atkinson, P. Acarnley, and J. Finch, "Observers for induction motor state and parameter estimation," *IEEE Trans. Ind. Appl.*, vol. 27, no. 6, pp. 1119–1127, Nov./Dec. 1991.
[12] R. Cuzner, R. Lorenz, and D. Novotny, "Application of nonlinear observers for rotor position detection on an induction motor using machine voltages and currents," in *Conf. Rec. IAS Annu. Meeting*, 1990, pp. 416–421. 90CH2935-5.
[13] K. Hurst, T. Habetler, G. Griva, F. Profumo, and P. Jansen, "A self-tuning, closed-loop flux observer for sensorless torque control of standard induction machines," in *Proc. IEEE Power Electron. Spec. Conf.*, 1995, pp. 792–798. 95CH35818.
[14] S. R. Sanders, "State estimation in induction machines," M.S. thesis, Mass. Inst. Technol., Cambridge, MA, Jun. 1985.
[15] S. R. Shaw and S. B. Leeb, "Identification of induction motor parameters from transient stator current measurements," *IEEE Trans. Ind. Electron.*, vol. 46, no. 1, pp. 139–149, Feb. 1999.
[16] S. R. Shaw, R. F. Lepard, S. B. Leeb, and C. R. Laughman, "A power quality prediction system," *IEEE Trans. Ind. Electron.*, vol. 47, no. 3, pp. 511–517, Jun. 2000.
[17] S. B. Leeb, U. A. Khan, and S. R. Shaw, "Multiprocessing transient event detector for use in a nonintrusive electrical load monitoring system," U.S. Patent 5 717 325, Feb. 10, 1998.
[18] S. B. Leeb and J. L. Kirtley, "Transient event detector for use in nonintrusive load monitoring systems," U.S. Patent 5 483 153, Jan. 9, 1996.
[19] G. W. Hart, "Nonintrusive appliance load monitoring," *Proc. IEEE*, vol. 80, no. 12, pp. 1870–1891, Dec. 1992.
[20] S. B. Leeb, "A conjoint pattern recognition approach to nonintrusive load monitoring," Ph.D. dissertation, Mass. Inst. Technol., Dept. Electr. Eng. Comput. Sci., Cambridge, MA, Feb. 1993.
[21] S. B. Leeb and S. R. Shaw, "Harmonic estimates for transient event detection," in *Proc. 29th Univ. Power Eng. Conf.*, 1994, pp. 133–166.
[22] R. W. Cox, "Minimally intrusive strategies for fault detection and energy monitoring," Ph.D. dissertation, Mass. Inst. Technol., Cambridge, MA, Sep. 2006.
[23] S. R. Shaw and C. R. Laughman, "A method for nonlinear least squares with structured residuals," *IEEE Trans. Autom. Control*, vol. 51, no. 10, pp. 1704–1708, Oct. 2006.
[24] S. R. Shaw, "Numerical methods for identification of induction motor parameters," M.S. thesis, Mass. Inst. Technol., Cambridge, MA, Feb. 1997.
[25] P. C. Krause, *Analysis of Electric Machinery*. New York: McGraw-Hill, 1986.
[26] T. DeNucci, R. Cox, S. B. Leeb, J. Paris, T. J. McCoy, C. R. Laughman, and W. C. Greene, "Diagnostic indicators for shipboard systems using non-intrusive load monitoring," in *Proc. IEEE Electr. Ship Technol. Symp.*, Philadelphia, PA, Jul. 2005, pp. 413–420.
[27] T. W. DeNucci, "Diagnostic indicators for shipboard systems using non-intrusive load monitoring," M.S. thesis, Mass. Inst. Technol., Cambridge, MA, 2005.

Steven R. Shaw (S'97–M'00–SM'05) received the Ph.D. degree in electrical engineering from the Massachusetts Institute of Technology, Cambridge, in 2000.

He is currently an Associate Professor with the Department of Electrical and Computer Engineering, Montana State University, Bozeman. His current research interests include sensors, instrumentation, modeling, and numerical and computational methods that are associated with control and measurement problems.

Steven B. Leeb (S'89–M'91–SM'01–F'07) received the Ph.D. degree in electrical engineering and computer science from the Massachusetts Institute of Technology (MIT), Cambridge, in 1993.

He is currently an Associate Professor with the Laboratory for Electromagnetic and Electronic Systems, Department of Electrical Engineering and Computer Science, MIT. His research interests include the design, analysis, development, and maintenance processes for all kinds of machinery with electrical actuators, sensors, or power electronic drives.

Leslie K. Norford received the Ph.D. degree in mechanical and aerospace engineering from Princeton University, Princeton, NJ, in 1984.

He is currently an Associate Professor of building technology with the Department of Architecture, Massachusetts Institute of Technology, Cambridge, where he has been a member of the faculty since 1988. His research interests include monitoring the performance of mechanical and electrical equipment in buildings, optimization techniques as applied to the design of buildings and their mechanical systems, simulation of the performance of building equipment, and efforts in support of sustainable buildings in developing countries.

Robert W. Cox (S'01–M'06) received the Ph.D. degree in electrical engineering and computer science from the Massachusetts Institute of Technology, Cambridge, in 2006.

He is currently an Assistant Professor with the Department of Electrical and Computer Engineering, University of North Carolina, Charlotte.